

A Novel H⁺ Conductance in Eosinophils: Unique Characteristics and Absence in Chronic Granulomatous Disease

By Botond Bánfi,^{*§} Jacques Schrenzel,^{* Oliver Nüsse,^{* Daniel P. Lew,^{* Erzsébet Ligeti,[§] Karl-Heinz Krause,[‡] and Nicolas Demaurex^{||}}}}

From the ^{*}Division of Infectious Diseases and [‡]Department of Geriatrics, Geneva University Hospitals, CH-1211 Geneva 4, Switzerland; the [§]Department of Physiology, Semmelweis Medical University, H-1444 Budapest, Hungary; and the ^{||}Department of Physiology, University of Geneva, CH-1211 Geneva 4, Switzerland

Summary

Efficient mechanisms of H⁺ ion extrusion are crucial for normal NADPH oxidase function. However, whether the NADPH oxidase—in analogy with mitochondrial cytochromes—has an inherent H⁺ channel activity remains uncertain: electrophysiological studies did not find altered H⁺ currents in cells from patients with chronic granulomatous disease (CGD), challenging earlier reports in intact cells. In this study, we describe the presence of two different types of H⁺ currents in human eosinophils. The “classical” H⁺ current had properties similar to previously described H⁺ conductances and was present in CGD cells. In contrast, the “novel” type of H⁺ current had not been described previously and displayed unique properties: (a) it was absent in cells from gp91- or p47-deficient CGD patients; (b) it was only observed under experimental conditions that allowed NADPH oxidase activation; (c) because of its low threshold of voltage activation, it allowed proton influx and cytosolic acidification; (d) it activated faster and deactivated with slower and distinct kinetics than the classical H⁺ currents; and (e) it was ~20-fold more sensitive to Zn²⁺ and was blocked by the histidine-reactive agent, diethylpyrocarbonate (DEPC). In summary, our results demonstrate that the NADPH oxidase or a closely associated protein provides a novel type of H⁺ conductance during phagocyte activation. The unique properties of this conductance suggest that its physiological function is not restricted to H⁺ extrusion and repolarization, but might include depolarization, pH-dependent signal termination, and determination of the phagosomal pH set point.

Key words: proton conductance • NADPH oxidase • granulomatous disease • hydrogen ion concentration • eosinophils

Phagocytes such as neutrophils, eosinophils, and macrophages kill invading pathogens by various mechanisms, including phagocytosis, secretion of proteolytic enzymes, and the production of toxic oxygen radicals (1–3). Superoxide is generated during the respiratory burst by the one-electron reduction of molecular oxygen, a reaction that is catalyzed by the NADPH oxidase complex (4, 5). This multicomponent enzyme is composed of at least two cytosolic subunits, p47^{phox} and p67^{phox}, and two membrane-associated subunits, p22^{phox} and gp91^{phox} (6, 7). Upon stimulation, the cytosolic components associate with the membrane-bound subunits, resulting in a functional NADPH oxidase. Patients with chronic granulomatous disease (CGD)¹ who have a missing or defective

subunit fail to assemble a functional oxidase and suffer from severe recurrent infections (8–10).

The assembled oxidase transfers electrons from cytosolic NADPH to extracellular oxygen (11, 12), a process that generates measurable currents across the plasma membrane (13). The electron transport can be sustained for several minutes, suggesting the existence of charge-compensating mechanisms (14). Efflux of H⁺ ions has long been postulated to provide the compensating charge (15), as large quantities of acid equivalents are generated in the cytosol during the respiratory burst (16, 17) and during the resynthesis of NADPH by the hexose monophosphate shunt (18). Despite this increased intracellular acid production, neutrophils alkalize during the respiratory burst, due in part to the concomitant activation of the Na⁺/H⁺ antiporter (19, 20). However, Na⁺/H⁺ exchange is electro-neutral and cannot provide a compensating charge (21). In contrast, H⁺ efflux through a conductive pathway would

¹Abbreviations used in this paper: CGD, chronic granulomatous disease; DEPC, diethylpyrocarbonate; DPI, diphenyliodonium; E_{H+} and E_{K+}, H⁺ and K⁺ equilibrium potential; E_{rev}, reversal potential of the current; pH_i, intracellular pH; pH_o, extracellular pH; TEACl, tetraethyl ammonium chloride.

provide an efficient mechanism of H⁺ extrusion and charge compensation.

H⁺ currents were initially described in snail neurons (22, 23) and subsequently found in many cellular systems (24, 25), including phagocytes (26–30). Common properties of proton conductances include voltage activation, regulation by intra- and extracellular pH, block by divalent cations, extremely high selectivity, high temperature dependency, and very small unitary conductance (for a review, see reference 31). Due to the lack of resolvable unitary events, H⁺ currents cannot be attributed unambiguously to ion channels, and we therefore prefer to use the term “conductance” (rather than “channel”) to describe an H⁺ permeation pathway that might involve a voltage-dependent ion carrier.

H⁺ conductance activity is highest in phagocytes, where it provides both a charge-compensating and a pH-regulating mechanism during the respiratory burst (32, 33). These cells express a plasma membrane cytochrome, gp91^{phox}, which, by analogy with mitochondrial cytochromes, has been proposed to function as an H⁺ channel (for a review, see reference 34). However, the experimental evidence regarding the H⁺ channel function of gp91^{phox} remains so far contradictory: (a) the NADPH oxidase and the H⁺ conductance have a similar pattern of activation by agonists (35, 36) and intracellular messengers (37, 38), and H⁺ currents develop in parallel with gp91^{phox} during the differentiation of HL-60 cells (39, 40). However, H⁺ currents are found in a variety of animal and human cells that do not express the phagocyte NADPH oxidase (22, 24, 41, 42). (b) Studies using pH-sensitive fluorescent dyes found signs of an abnormal H⁺ conductance in TPA- or AA-stimulated CGD cells (40, 43, 44). However, a patch clamp study reported normal H⁺ current in monocytes from patients with X-linked CGD, who completely lacked the gp91^{phox} subunit (45). Nevertheless, transfection of gp91^{phox} into Chinese hamster ovary (CHO) fibroblasts conferred H⁺ conductance to these NADPH oxidase-negative cells (40, 46).

To clarify the role of the NADPH oxidase in proton transport, we used human eosinophils, whose oxidase activity can be readily measured with the patch clamp technique (13). This enabled us to demonstrate for the first time that CGD patients lack an oxidase-associated H⁺ conductance that is activated during the respiratory burst.

Materials and Methods

Patients. The gp91^{phox}-negative CGD patient was a 6-yr-old Caucasian boy. The p47^{phox}-negative CGD patient was a 34-yr-old Caucasian woman. Both patients had been thoroughly documented and completely lacked the respective oxidase subunits.

Materials and Media. Tetraethyl ammonium chloride (TEACl), 2-(*N*-morpholino)ethanesulfonic acid (MES), Hepes, diethylpyrocarbonate (DEPC), and Tris were from Sigma Chemical Co. The pH-sensitive fluorescent dye 5'-(and 6')-carboxy-10-dimethylamino-3-hydroxy-spiro[7H-benzo[*c*]xanthene-7,1'(3'H)-isobenzofuran]-3'-one (carboxy-SNARF-1, free and acetoxymethylester form) was purchased from Molecular Probes, Inc. All other chemicals were of analytical grade and obtained from Sigma Chemical Co., Merck, or Fluka.

Unless otherwise indicated, the recording solutions used in current measurements contained (in mM) CsCl 75, CsOH 50, TEACl 10, MgCl₂ 1, buffered to the indicated pH with 50 mM of MES (pH 6.1 and 6.6), Hepes (pH 7.1–7.6), or Tris (pH 8.1). In addition, the bath solution contained 0.1% glucose, and the pipette solution 1 mM MgATP and 8 mM NADPH. Free Ca²⁺ concentration was ~5 μM, measured with a calcium electrode (13). The quasiphysiological solutions used for some membrane potential measurements were buffered as described above and contained (in mM), pipette: KCl 110, NaCl 5, KOH 2.4, MgCl₂ 2; bath: NaCl 109, NaOH 2.4, KCl 5, MgCl₂ 2, 0.1% glucose. DEPC was dissolved in 50% ethanol at 1.2 M and used at a final concentration of 1.2 mM, such that the final ethanol concentration did not exceed 0.1%. The various free Zn²⁺ concentrations used in Fig. 7, A and B, were buffered by citrate (5 mM) according to calculations performed with the MaxChelator 6.7 program (Chris Patton, Stanford University, Stanford, CA).

Cells. Human eosinophils (>98% pure) were isolated from heparinized or citrated whole blood obtained by venipuncture, using dextran sedimentation, discontinuous plasma-Percoll gradients, and negative selection by CD16-coupled magnetic beads as described (30). The same procedure was used to obtain eosinophils from CGD patients. After isolation, cells were kept on ice until used (generally <10 h). All experiments were performed at room temperature. Oxygen depletion was performed as described (13).

Measurements of Cytosolic pH. Cytosolic pH was measured with the dual emission pH indicator carboxy-SNARF-1, as described previously (26), using an inverted microscope (Nikon Diaphot) equipped with a xenon arc lamp and the appropriate filters (Glen Spectra Ltd.). The fluorescence intensity at 580 and 640 nm was measured simultaneously on two photometers (Hamamatsu) and recorded at a rate of 50 Hz using a 12-bit A/D converter (Acqui; Sicomu). Eosinophils were incubated with 5 μM carboxy-SNARF-1 acetoxymethylester for 30 min at room temperature just before recordings in the whole cell patch clamp configuration. To compensate for the diffusion of the dye into the patch pipette, 100 μM carboxy-SNARF-1 (free acid) was included in the pipette solution. Data are expressed as the ratio of carboxy-SNARF-1 640 nm to 580 nm emission.

Patch Clamp Recordings. The whole cell patch clamp technique (47) was used to measure whole cell membrane currents and membrane potential, essentially as described (26, 30). Patch pipettes were pulled from borosilicate glass (1.5 mM OD; Clark Electromedical Instruments) using a Flaming Brown automatic pipette puller (Sutter Instruments). Pipettes were fire-polished and had resistance in the range of 3–12 MΩ; seal resistance was 5–50 GΩ. Patch recordings were performed using a Axopatch 200A amplifier (Axon Instruments), in the current clamp or voltage clamp mode. Values for whole cell resistance varied between 2.5 and 30 GΩ; mean access resistance was between 10 and 30 MΩ. Cell capacitance ranged from 1.8 to 3.0 pF. Data were low-pass filtered at 20 Hz through an eight-pole Bessel filter and digitized at 100 Hz on a 12-bit A/D converter (Acqui; Sicomu), which also provided the voltage pulses. In addition, all experiments were recorded at high frequency (44 kHz) on a DAT tape recorder (DTR 1801; Biologic). Leak currents were small compared with the studied currents, and were subtracted only to calculate the current-voltage relationship of the time-dependent currents. Traces shown are not corrected for leak current and were smoothed by averaging 5 or 40 consecutive data points. In ~30% of the cells, a transient (<10 s) outward current (presumably carried by K⁺) developed immediately after break-in (e.g., see Fig. 5 A, bottom left trace); this current was observed in both control and CGD cells.

Data Analysis. The recorded traces, filtered at 500 Hz, were digitized at 2 kHz and transferred to Origin software for analysis (MicroCal). For tail current analysis, exponential curves were fitted to the deactivating currents using the Origin software. To avoid capacitance artifacts, the first 5 ms after the repolarization were not considered for analysis. Computation required ~ 20 – 200 iterations to reach a stable condition with a level of confidence of 1%, as assessed by the nonlinear least squares regression method.

Results

An H^+ Conductance Sets the Membrane Potential during the Respiratory Burst. To investigate the role of the H^+ conductance during the respiratory burst, we directly measured changes in membrane potential during activation of eosinophils from control and CGD patients, using the current clamp mode of the patch clamp technique. Electron transfer through the NADPH oxidase is electrogenic and is associated with a depolarization of the plasma membrane (15, 33). The magnitude of this depolarization is unknown but likely exceeds the threshold of activation of the phagocytic H^+ conductance, since conductive H^+ efflux has been reported during the respiratory burst (36). We took advantage of the patch clamp technique to activate the oxidase, by including its substrate NADPH together with Ca^{2+} and/or nonhydrolyzable GTP analogues in the patch pipette (13; see also Fig. 2 A).

In initial experiments, 125 mM Cs^+ and 10 mM TEA were included in the solutions to block the inwardly rectifying K^+ channel of eosinophils (Kir 2.1), which normally sets the membrane potential close to the K^+ equilibrium potential (E_{K^+}) (48). As shown in Fig. 1 A, control eosinophils rapidly depolarized upon perfusion with a pipette

containing 25 μM GTP γS (arrowhead). The time course of the membrane potential changes was biphasic: the cells depolarized within 30 s and then repolarized to approximately +30 mV, i.e., close to the H^+ equilibrium potential ($E_{H^+} = +29$ mV). Addition of Zn^{2+} (10 μM), a known blocker of the phagocytic H^+ conductance, caused the cells to depolarize to extremely high values (+80 mV). This suggested that, at the steady state +30 mV potential, an H^+ conductance was counteracting the depolarization induced by the oxidase.

To assess the contribution of the H^+ conductance, we measured membrane potential changes at various bath and pipette pH. As shown in Fig. 1 B, the amplitude of the depolarization increased when the external pH was made more acidic than the cytosol, whereas the cells hyperpolarized when the pH gradient was reversed. A plot of the steady state membrane potential against the pH gradient (Fig. 1 C) revealed that the membrane potential of activated eosinophils (upward triangles) closely followed the H^+ equilibrium potential (dotted line). Identical values were obtained when the experiments were repeated in quasiphysiological solutions devoid of TEA (downward triangles), suggesting that the contribution of K^+ channels was minimal. However, regardless of the pH gradient, the cells depolarized to approximately +80 mV upon addition of Zn^{2+} (filled triangles). This confirmed that an H^+ conductance was equilibrating the membrane potential with the pH gradient.

In contrast, cells from a p47-deficient CGD patient, which lacked a functional oxidase, failed to depolarize and remained insensitive to Zn^{2+} (Fig. 1 A, bottom trace). As shown in Fig. 1 C, the CGD cells maintained a negative potential at all pH (open circles), even in the presence of

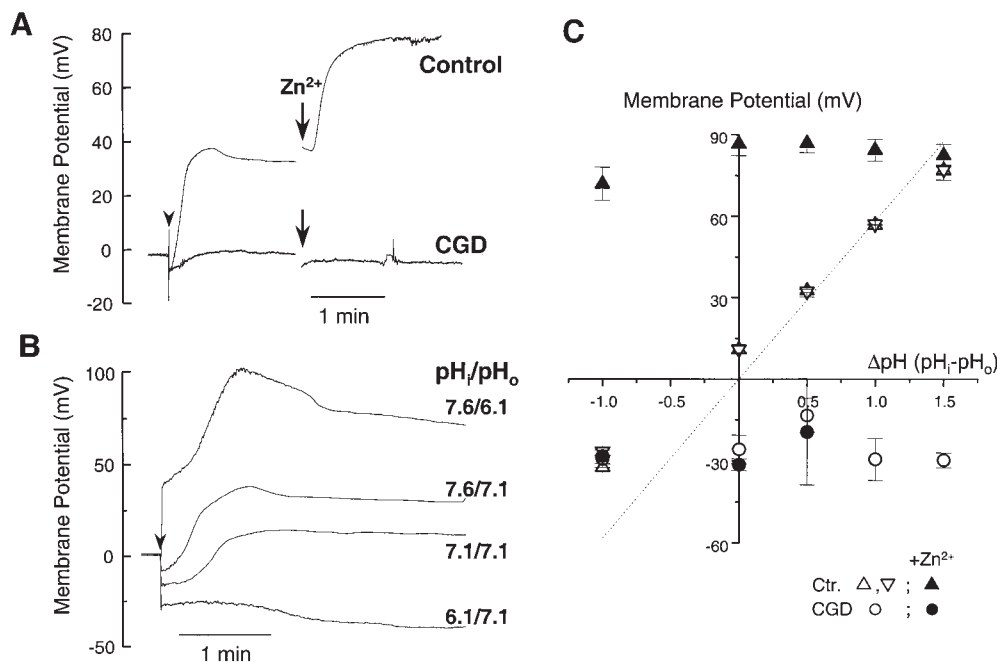


Figure 1. Membrane potential changes during activation of control and CGD eosinophils. The membrane potential of eosinophils, determined as the zero current holding potential, was measured in current clamp mode after the formation of the whole cell configuration (arrowhead). The pipette solutions contained 8 mM NADPH and 25 μM GTP γS to activate the oxidase. (A) Time course of the membrane potential changes in control and CGD eosinophils, measured in Cs^+ -based solutions containing 10 mM TEA ($pH_i = 7.6$, $pH_o = 7.1$). When indicated, the H^+ conductance blocker, Zn^{2+} (10 μM), was added to the bath solution. (B) Membrane potential changes measured with $CsCl$ solutions buffered to different pH. (C) The steady state membrane potential of control (triangles) and CGD cells (circles) is plotted against the transmembrane pH gradient, measured in $CsCl$ (upward triangles) or quasiphysiological (downward triangles) solutions, in the absence (open symbols) or presence (filled symbols) of Zn^{2+} . The dotted line represents the calculated H^+ equilibrium potential. Data are mean \pm SEM of ≥ 5 experiments for each condition.

Zn²⁺ (filled circles). This demonstrated that a functional oxidase is required not only for the depolarization, but also for the activation of an H⁺ conductance. The H⁺ conductance then counteracted the depolarization and rendered the cell pH sensitive, setting the membrane potential according to the pH gradient. This latter observation was surprising, inasmuch as the known H⁺ conductances open at voltages significantly higher than E_{H⁺} (49). Thus, the H⁺ conductance activated during the respiratory burst appeared to have an unusually low threshold of activation.

Activation of the Oxidase Is Associated with Inward H⁺ Currents. To investigate the unusual behavior of this H⁺ conductance, we directly measured proton currents during the respiratory burst in voltage-clamped experiments. To vary the degree of oxidase activation, we perfused calcium chelators or GTP analogues through the patch pipette. As described previously (13), electron transport by the oxidase generated inward currents that developed slowly upon cell activation (Fig. 2 A, left traces). These electron currents were sustained for several minutes (*n* = 804) and did not display time-dependent voltage activation or inactivation, allowing concomitant recordings of currents elicited by depolarizing voltage steps (Fig. 2 A, right traces).

As shown in Fig. 2 A, perfusion of eosinophils with ~5 μM unbuffered free [Ca²⁺] generated an electron current whose amplitude, 2 min after achieving the whole cell configuration, averaged -3.9 ± 0.16 pA/pF (*n* = 32). Despite the use of alkaline pipette solutions to minimize H⁺ currents (intracellular pH [pH_i] 7.6, extracellular pH [pH_o] 7.1), voltage-activated outward currents were observed above +30 mV (E_{H⁺} = +29 mV), whereas deactivating tail currents (current observed after stepping back to the holding voltage) were observed above 0 mV (Fig. 2 A, top right traces). This suggested that an ionic conductance was already activated at 0 mV, yet produced measurable steady state currents only at higher voltages. To quantitate the amplitudes of the voltage-activated currents, the currents measured 500 ms after the beginning of the voltage pulse were subtracted from the current measured at the end of the 5-s pulse, and the result was plotted against the activating voltage (Fig. 2 B). The current-voltage relationship revealed that small (-1.3 ± 0.2 pA, *n* = 12) inward current developed already at voltages higher than 0 mV (Fig. 2 B, circles). This current reversed sign close to the H⁺ equilibrium potential (E_{rev} = +30 mV, E_{H⁺} = +29 mV), suggesting that it might be carried by H⁺ ions. Furthermore, its slow kinetics of voltage activation and deactivation were similar to previously described H⁺ currents. However, this putative H⁺ current activated well below the expected voltage range for the H⁺ conductance of phagocytes, which has been thought to carry only outward H⁺ current.

This unusually low threshold of activation was not observed in conditions that prevented oxidase activation, i.e., calcium buffered with 10 mM EGTA (electron current density, 2 min after break-in, -1.0 ± 0.22 pA/pF; *n* = 11). Under those conditions, little or no current was elicited by depolarizing pulses (Fig. 2 A, middle traces), and the I-V curve revealed only small outward currents that activated at voltages

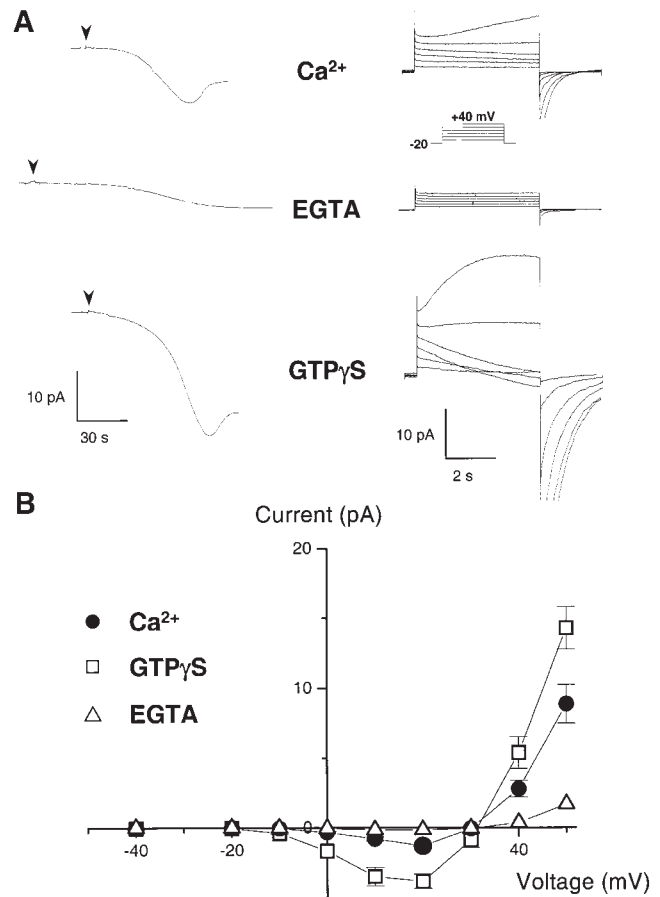


Figure 2. H⁺ currents during activation of the NADPH oxidase. (A) Whole cell current in human eosinophils measured under resting and stimulated conditions. The pipette solution contained 8 mM NADPH to provide substrate for the oxidase, and either no calcium buffer (top, ~5 μM free [Ca²⁺]), 10 mM EGTA (middle), or 25 μM GTPγS (bottom). After break-in (arrowheads), the electron currents were recorded at 0 mV (left traces). After achieving a steady state, the holding voltage was changed to -20 mV, and 5-s depolarizing steps ranging from -10 to +40 mV (inset) were applied in 10-mV increments to elicit H⁺ currents (right traces). Traces are representative of ≥20 experiments for each condition. (B) Current-voltage plot of the voltage-dependent currents measured with ~5 μM free [Ca²⁺] (●), 25 μM GTPγS (□), and 10 mM EGTA (△). Currents measured 500 ms after the beginning of a 5-s-long voltage pulse were subtracted from the current measured at the end of the pulse. The leak-subtracted currents reversed sign around +30 mV, close to the H⁺ reversal potential (pH_i = 7.6, pH_o = 7.1; E_{H⁺} = +29 mV; mean ± SEM of ≥7 experiments).

higher than +40 mV (Fig. 2 B, triangles) consistent with the known behavior of the H⁺ conductance (29, 30). This suggested that the degree of cellular activation and/or the concomitant activation of the NADPH oxidase could alter the voltage dependence of the H⁺ conductance of phagocytes.

To test this possibility, we perfused GTPγS through the patch pipette to induce maximal cell activation and stimulate the respiratory burst. GTPγS increased the amplitude of the electron currents (-7.5 ± 0.3 pA/pF, *n* = 36), confirming that the oxidase was strongly activated (Fig. 2 A, bottom left trace). Under these conditions, the amplitude of the voltage-activated currents was markedly increased (Fig. 2 A, bottom right traces), and the threshold of voltage

activation was shifted to even lower values (Fig. 2 B, squares). Thus, activation of the oxidase was associated with large voltage-dependent currents that activated well below the H^+ equilibrium potential. Given the kinetic similarities with the known H^+ currents of phagocytes and the fact that, in our ionic conditions, H^+ was the only known permeant ion, the observed current was likely carried by H^+ . This suggested that, upon oxidase activation, the threshold of voltage activation of the H^+ conductance was shifted below E_{H^+} , allowing H^+ ions to enter the cell down their electrochemical gradient.

pH Changes Associated with the Inward Current. To demonstrate that the inward current observed in activated eosinophils was carried by H^+ ions, we measured the cytosolic pH changes during depolarizing voltage steps (Fig. 3 A). The cells were loaded with the pH-sensitive fluorescent indicator carboxy-SNARF-1, and changes in pH_i were measured by ratio emission photometry. After break-in (arrow), a robust e^- current developed, and the cell alkalinized as it equilibrated with the pipette solution (pH 7.6). After the establishment of a steady state pH and current, long-lasting depolarizing voltage steps were applied to elicit the voltage-dependent inward current. As shown in Fig. 3 A, depolarizing steps to +20 mV (middle trace) elicited large inward currents (bottom trace) that were accompanied by a sizable cytosolic acidification (top trace). The current rapidly deactivated upon repolarization to -20 mV, and the cell realkalinized as base equivalents were continuously perfused through the patch pipette. Addition of Zn^{2+} , which blocks H^+ currents in several cell types, abolished both the pH_i changes and the associated inward currents (Fig. 3 A).

This confirmed that the inward current was carried by H^+ ions, and suggested that the underlying conductive pathway might be the Zn^{2+} -sensitive H^+ conductance of phagocytes.

As, under our activating conditions, the H^+ conductance is open below and above E_{H^+} , it is expected to drive both cytosolic acidification and alkalinization depending on the driving force for H^+ ions. To test this possibility, a depolarization was applied to elicit outward current, and the external medium was exchanged for a more acidic solution to change the direction of the protonmotive force (Fig. 3 B). As expected, the outward current was associated with a large cytosolic alkalinization, whereas after the change of the pH_o from 7.1 to 6.6, the cell rapidly acidified (Fig. 3 B, top). This cytosolic acidification was associated with a large inward current (Fig. 3 B, bottom) that rapidly inactivated, likely reflecting the reduction in the H^+ driving force as the cytosolic pH decreased. Thus, at constant voltage, the H^+ conductance can drive either cytosolic alkalinization or acidification after changes in the pH gradient.

Modulation of the H^+ Currents by pH_i . The direction of the H^+ flux at constant voltage could also be reversed when different pH_i were imposed through the patch pipette (Fig. 4). Reducing the pipette pH from 7.6 to 7.1 changed the direction of the H^+ current at +10 mV (Fig. 4 A) and shifted the reversal potential of the current by -30 mV (Fig. 4 B). Conversely, increasing pH_i by 0.5 pH unit shifted the reversal potential of the current by +30 mV (Fig. 4 B). In each case, the reversal potential of the current was close to the H^+ equilibrium potential (arrows), confirming that the inward and outward currents were carried by H^+ ions. In addition to the expected changes in the reversal potential,

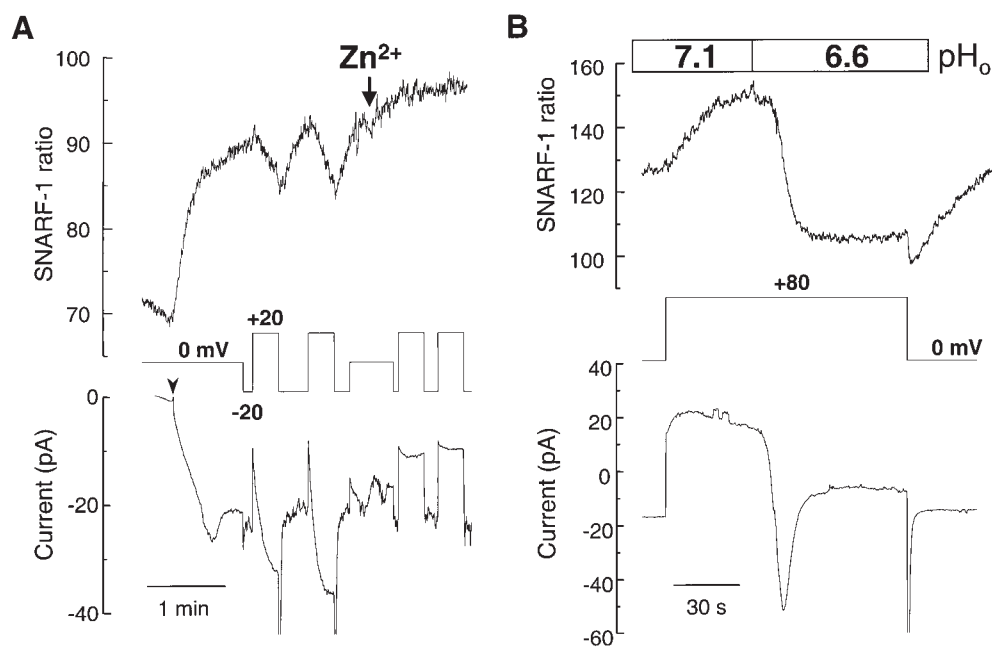


Figure 3. H^+ current-associated changes in cytosolic pH. Combined recordings of whole cell currents and cytosolic pH changes measured with the fluorescent pH indicator carboxy-SNARF-1. The pipette solutions contained 25 μ M GTP γ S and 8 mM NADPH. (A) After break-in (arrowhead), the cytosol was allowed to equilibrate with the alkaline pipette solution (pH = 7.6). Then, long-lasting (20 s) depolarizing steps to +20 mV were applied (middle), and the currents (bottom) and cytosolic pH changes (top) were measured concomitantly. When indicated, Zn^{2+} (10 μ M) was added to the bath solution. (B) A sustained depolarization to +80 mV was imposed (middle) to allow H^+ efflux through the conductance ($pH_i = 8.1$, $pH_o = 7.1$, $E_{H^+} = +58$ mV). After establishing a new steady state pH (top) and current (bottom), the external pH was rapidly decreased from 7.1 to 6.6 to change the direction of the H^+ gradient ($E_{H^+} = +90$ mV). Recordings are representative of ≥ 16 experiments for each condition.

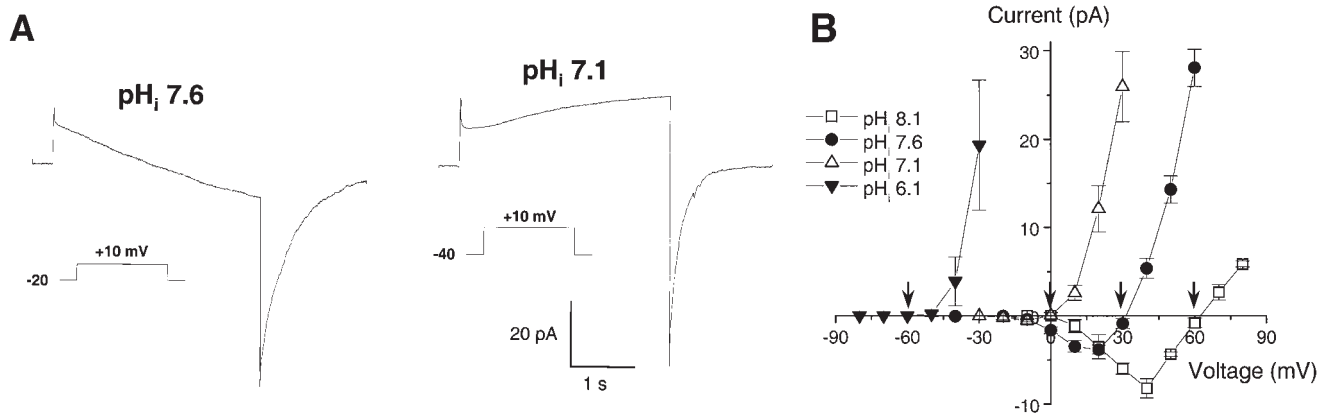


Figure 4. pH dependence of the H⁺ currents. (A) Currents elicited by a 5-s depolarizing pulse to +10 mV in cells perfused with alkaline (pH = 7.6, $n = 20$) or neutral (pH = 7.1, $n = 7$) pipette solutions containing 25 μ M GTP γ S. (B) Current-voltage relationship measured at a pipette pH of 6.1 (\blacktriangledown), 7.1 (\triangle), 7.6 (\bullet), and 8.1 (\square). The holding voltage was -60 mV (pH 6.1), -40 mV (pH 7.1), and -20 mV (pH 7.6 and 8.1), and bath pH was 7.1 in all conditions. Arrows indicate the H⁺ equilibrium potential for each condition. Data are mean \pm SEM of ≥ 7 experiments for each condition.

changing the transmembrane pH gradient shifted the threshold of voltage activation of the H⁺ current (Fig. 4 B). At neutral or alkaline pH_i, the current activated well below the H⁺ equilibrium potential, thus producing inward H⁺ currents (Fig. 4 B, squares and circles). In contrast, at acidic pH_i the current activated above the reversal potential, and only outward H⁺ currents were observed (Fig. 4 B, downward triangles).

Thus, the low threshold of activation observed in activated eosinophils is lost at acidic pH_i. The loss was not due to a decrease in oxidase activity, since a positive NBT stain was observed at pH_i 6.1 (not shown) and the amplitude of electron currents was similar when measured in acidic or alkaline solutions (-7.64 ± 1.03 vs. -7.5 ± 0.3 pA/pF, $n = 8$ and 36, respectively). This apparent inhibition

at acidic pH_i differs from the known properties of H⁺ conductances, which activate at acidic pH_i.

The Inward H⁺ Current Is Not Coupled to Electron Transport. The development of inward H⁺ currents closely correlated with the amplitude of electron transfer by the oxidase (Fig. 2 A), suggesting coupling between electron and proton transport. To test this hypothesis, we measured the H⁺ currents under conditions that allowed the assembly of the oxidase, but prevented its redox function. As shown in Fig. 5 A, block of electron transport by diphenyliodonium (DPI) or removal of oxygen, the electron acceptor, from the bath solution, completely abolished the electron current through the oxidase (left traces). The electron current density was smaller than -0.5 pA/pF in both cases ($n = 19$ and 14 for DPI and oxygen-depleted, respectively).

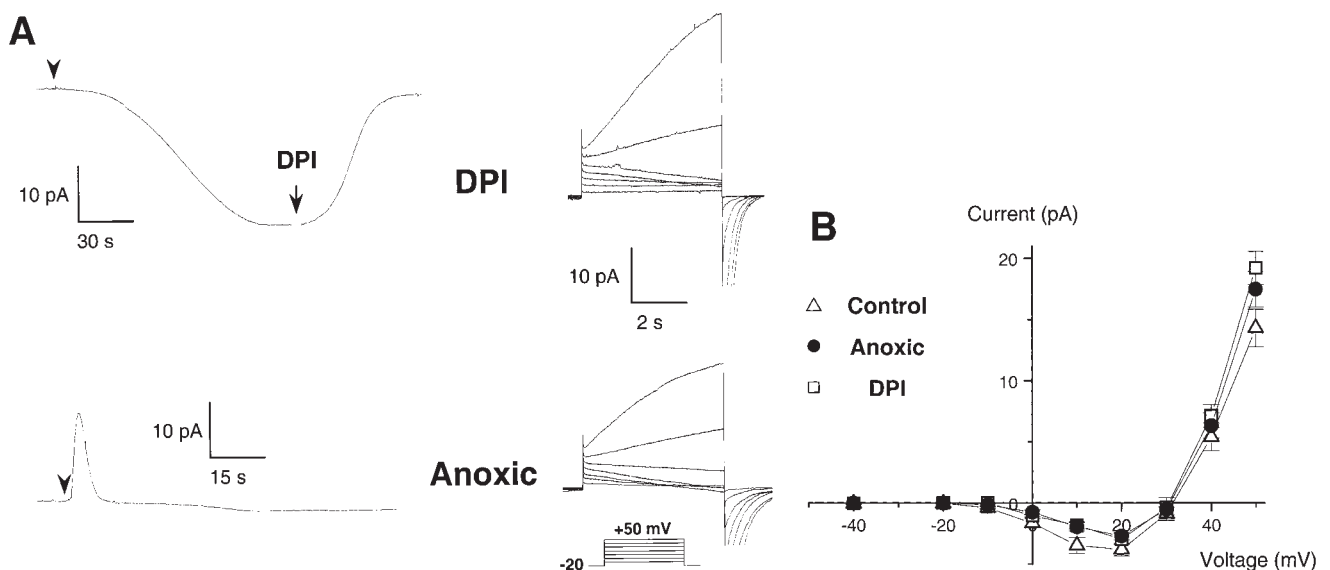


Figure 5. The inward H⁺ currents do not require oxidase activity. (A) Effect of DPI (top) and of oxygen depletion (bottom) on the electron (left) and proton currents (right traces). Pipette solutions contained 25 μ M GTP γ S, 8 mM NADPH, pH 7.6; bath pH 7.1. Oxygen was removed from the bath solution by a 4-h preincubation with glucose-oxidase (50 mU/ml) and catalase (2,000 U/ml). Traces are representative of ≥ 7 experiments. (B) Current-voltage relationship of the H⁺ currents, measured as in the legend to Fig. 2, under control conditions (\triangle , $PO_2 = 25.7 \pm 0.3$ kPa), in the presence of DPI (\square), or under low oxygen conditions (\bullet , $PO_2 < 1$ kPa). Data are mean \pm SEM of ≥ 7 experiments for each condition.

However, neither procedure had major effects on the H⁺ currents (right traces). The slight reduction in the amplitude of the inward currents (Fig. 4 B) was not statistically significant ($P > 0.05$). Thus, the inward H⁺ current is not coupled to electron transport and does not require concomitant oxidase activity.

The Inward H⁺ Current Is Absent in CGD Patients. Although the inward H⁺ currents did not require electron flow through the oxidase, they were only observed in conditions favoring oxidase assembly, suggesting a close coupling between the two systems. To analyze in detail the molecular basis of this putative interaction, we measured the currents in two patients with CGD. One patient had X-linked CGD and was completely deficient in the transmembrane gp91^{phox} subunit of the oxidase, whereas the second patient lacked the cytosolic p47 subunit. As expected, eosinophils from these CGD patients did not produce a detectable amount of superoxide and failed to generate electron currents upon activation with GTP γ S (not shown). As shown in Fig. 6 A, the two types of CGD cells were completely devoid of inward H⁺ currents (top traces). However, small outward currents were observed in both the gp91- and p47-deficient cells, suggesting that an H⁺ conductance was present in the CGD cells. Accordingly, when measured in the acidic conditions classically used for H⁺ current detection (pH_i 6.1, 0.2 mM EGTA), CGD eosinophils had near-normal H⁺ currents (right traces). Thus, an H⁺ conductance is present and functional in CGD cells, but is unable to catalyze H⁺ influx in response to cell activation. This abnormal behavior was not due to a lack of response to GTP γ S or Ca²⁺, which had a marked effect on the outward H⁺ currents (Fig. 6 C). Despite the activation, however, GTP γ S and Ca²⁺ did not induce the apparition of inward currents (compare Fig. 6 C with Fig. 2 B). Thus,

CGD cells possess an endogenous H⁺ conductance distinct from gp91^{phox}, which can be activated by cytosolic acidification, by Ca²⁺, and by GTP γ S. However, regardless of the mode of activation, this conductance carries only outward current in CGD cells.

Eosinophils Express Two Distinct H⁺ Conductances. The absence of inward H⁺ current in CGD eosinophils could result from the defective modulation of a preexisting, outward-rectifying H⁺ conductance. Alternatively, it could reflect the lack of a distinct H⁺ entry pathway linked to one of the oxidase subunits. To distinguish between these two possibilities, we analyzed in detail the kinetic and pharmacological properties of the inward and outward H⁺ currents. Polyvalent metal cations such as Cd²⁺ and Zn²⁺ block, at submillimolar concentrations, all the voltage-activated H⁺ currents described to date (31, 32). The block is voltage dependent and mimics a lowering in pH_o, suggesting that the cations interact with the external H⁺ binding site on the transport protein (50). If a separate conductance with a higher affinity for external H⁺ is activated, the resulting currents should thus be more sensitive to block by Cd²⁺ and Zn²⁺. Consistent with this hypothesis, a large fraction of the outward currents observed in control, activated eosinophils was already blocked by submicromolar concentrations of Zn²⁺, whereas higher concentrations were required to block the residual currents (Fig. 7 A). Accordingly, the dose-inhibition curve of the outward currents was biphasic, with apparent K_D of 150 nM and 2.4 μ M, suggesting the presence of both a high-affinity and a low-affinity conductance (Fig. 7 B, open circles). In contrast, the dose-inhibition curve of the inward currents was monophasic, with an apparent K_D of 133 nM, consistent with the presence of only a single, high-affinity conductance (Fig. 7 B, open circles). Thus, two H⁺ conductances with distinct

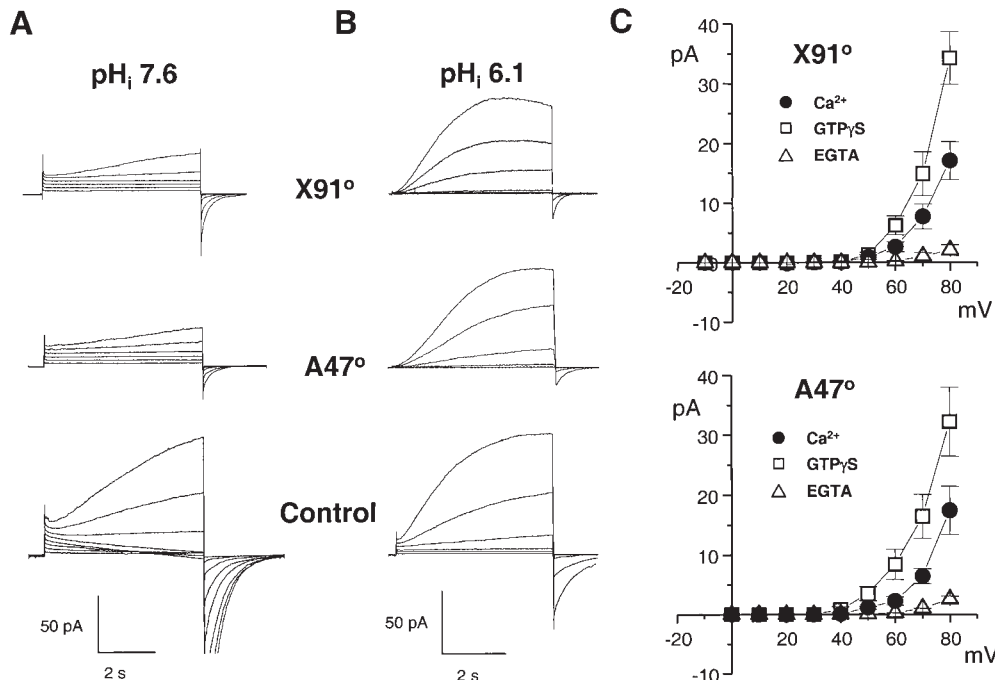


Figure 6. The inward H⁺ currents are absent in CGD patients. Proton currents recorded in eosinophils from two CGD patients: a 6-yr-old Caucasian boy with X-linked CGD, who completely lacked the gp91^{phox} subunit (X91°), and a 34-yr-old Caucasian woman with a deficiency in p47 (A47°). (A) Families of currents elicited by 5-s depolarizing steps ranging from 0 mV (CGD) or -20 mV (Control) to +50 mV, in conditions favoring inward currents (pH_i = 7.6, 25 μ M GTP γ S). (B) Currents elicited by 5-s pulses from -60 mV to 0 mV, in conditions minimizing inward currents (pH_i 6.1, 0.2 mM EGTA, no GTP γ S). Traces are representative of ≥ 8 experiments. (C) Current-voltage plot of proton currents measured in CGD cells under different activating conditions (pH_i = 7.6, pH_o = 7.1). Data are mean \pm SEM of ≥ 4 experiments for each condition.

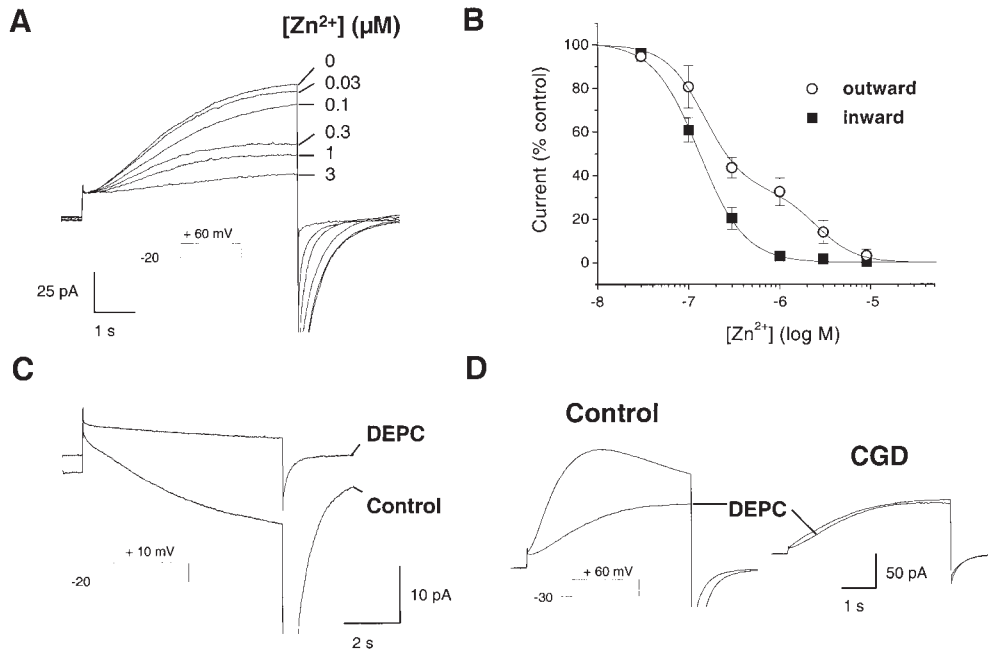


Figure 7. Block of the currents by Zn^{2+} and DEPC. Effect of the polyvalent cation Zn^{2+} and of the histidine reagent DEPC on the H^+ currents of control and CGD cells. Pipette solutions contained 25 μ M GTP- γ S, pH_i 7.6 (A–C) or 7.1 (D), pH_o 7.1. (A) Effect of Zn^{2+} on the outward currents in control, activated eosinophils. Currents were elicited by a pulse from -20 to $+60$ mV, and increasing free concentrations of Zn^{2+} (buffered with 5 mM citrate) were added to the bath solution. Traces are representative of ≥ 11 experiments. (B) Dose-inhibition curves of the block by Zn^{2+} . The fractional outward (\circ , measured at $+60$ mV) or inward (\blacksquare , measured at $+20$ mV) current is plotted against the extracellular Zn^{2+} concentration. Data are mean \pm SEM of ≥ 4 experiments for each condition, fitted with a single (\blacksquare) or double sigmoidal

curve (\circ) using Origin software. (C) Effect of DEPC (1.2 mM) on the inward current induced by a 7-s-long depolarization to $+10$ mV. (D) Effect of DEPC on the outward current induced by a 5-s depolarization to $+60$ mV. Traces are representative of ≥ 7 experiments.

Zn^{2+} sensitivity appeared to coexist in activated eosinophils. The low-affinity component likely reflected the endogenous H^+ conductance which, in a previous study using nonactivated eosinophils, was blocked by Zn^{2+} with a half-inhibitory concentration of 4 μ M (30).

To verify that the high-affinity component reflected the activation of a separate conductance, we searched for organic inhibitors able to block the inward H^+ currents. Since several H^+ conducting transporters contain histidyl residues, whose protonation/deprotonation play a key role in H^+ translocation (51–53), we tested the effects of DEPC, a histidine-modifying reagent. DEPC did not significantly affect the activity of the oxidase, as it reduced the amplitude of electron currents by only $2.57 \pm 0.04\%$ ($P = 0.56$, $n = 22$). DEPC specifically reacts with histidyl residues at physiological pH (54–56), and is thus expected to affect the currents if histidine residue(s) are involved in either inward or outward proton transport. As shown in Fig. 7 C, DEPC almost completely blocked the inward H^+ current. In contrast, DEPC had no effects on the outward H^+ current of CGD eosinophils, and only partially blocked the outward H^+ current in control cells (Fig. 7 D). This suggested that histidine residue(s) are critical for the inward H^+ currents, and mediate part of the outward H^+ current observed in control cells. In contrast, histidine residues are either not accessible for DEPC or not involved in outward H^+ transport by CGD eosinophils.

To confirm the existence of two separate H^+ conductive pathways, we analyzed in detail the kinetics of activation and deactivation of the currents. As shown in Fig. 8 A, superimposition of the currents elicited by a pulse to $+60$ mV and normalized to the peak current measured at this volt-

age revealed that current activation was more rapid in control than in CGD cells. Addition of DEPC, which had no effect on CGD cells (Fig. 7 D), slowed current activation to levels comparable to CGD cells (Fig. 8 A). At all voltages, the time for half-maximal activation ($t_{1/2}$ act, measured by fitting a sigmoidal curve to the current) was significantly lower in control cells, and increased to values comparable to CGD cells upon addition of DEPC (Fig. 8 B).

To study the kinetics of deactivation, outward H^+ currents of similar magnitudes were induced by depolarizing the cells to $+60$ mV for different duration, and the tail currents measured at different deactivating voltages were compared. As shown in Fig. 8 C, current deactivation was much slower in control than in CGD eosinophils. Addition of DEPC, which had no effects in CDG cells (Fig. 7 D), dramatically accelerated current deactivation in control cells (Fig. 8 C). To check whether the slow deactivation was due to a distinct conductance, we attempted to fit the tail currents with multiple exponential components. The tail currents of CGD cells were best fitted with a double exponential, with time constants at -20 mV of $\tau_1 = 34.6 \pm 5.39$ and $\tau_2 = 201.78 \pm 52.8$ ms. Attempting to fit a third exponential component did not significantly improve the fit quality ($P = 0.448$). In contrast, the tail currents of control cells were fitted significantly better when a third exponential, with time constant of $\tau_3 = 1,301.88 \pm 169.95$ ms, was included in the fitting procedure ($P < 0.002$ by χ^2 analysis). This slow, additional component was observed within the whole tested voltage range and was more sensitive to voltage than the two faster components (Fig. 8 D). Addition of DEPC reduced the amplitude of the slow component by 84.6%, but had only marginal effects on the

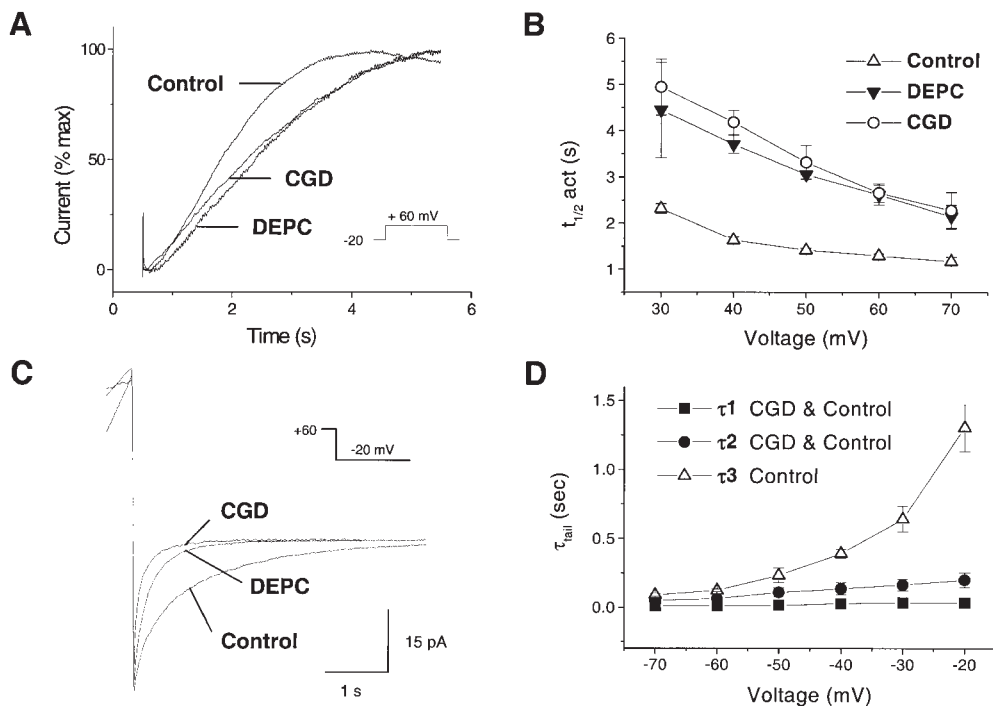


Figure 8. Activation and deactivation of the currents in control and CGD cells. pH_i 7.1 (A, B) or 7.6 (C, D), pH_o 7.1. (A) Kinetics of current activation in control, CGD, and DEPC-treated cells. Currents elicited by a 5-s-long pulse from -20 mV to +60 mV were normalized to the maximal current recorded at this voltage and superimposed for comparison. (B) Voltage dependence of current activation. The time for half-maximal activation ($t_{1/2 \text{ act}}$) is plotted against the activating voltage. (C) Kinetics of current deactivation during repolarization from +60 mV to -20 mV. Cells were depolarized for various durations to induce currents of similar amplitude. Traces are representative of ≥ 9 experiments. (D) Voltage dependence of the deactivation time constants (τ_{tail}), estimated by fitting exponential curves to the currents measured after a pulse to +60 mV. The two fast kinetic components (τ_1 , ■; τ_2 , ●) are present in both control and CGD cells, whereas an additional third slow component (τ_3 , △) is absent from CGD cells. Data are mean \pm SEM of ≥ 5 experiments for each condition.

amplitude of the two fast components observed in control and CGD cells (not illustrated). Thus, H⁺ currents in activated eosinophils had an additional component that could be blocked by DEPC, unmasking slowly activating, rapidly deactivating currents that were indistinguishable from the currents observed in CGD cells.

These results are best compatible with the coexistence of two separate H⁺ conductive pathways (Fig. 9). One conductance, present in both control and CGD cells, activates slowly, inactivates rapidly, is blocked by Zn²⁺ with low affinity, and is insensitive to DEPC. In addition, a conductance coupled to the oxidase is absent in CGD, activates rapidly, inactivates slowly, is highly sensitive to Zn²⁺, and is blocked by DEPC.

Discussion

In this study, we describe a novel type of H⁺ current associated with the activation of the NADPH oxidase in human eosinophils. The current was absent in cells from either gp91- or p47-deficient CGD patients, and developed on top of outward-rectifying H⁺ currents that were present in both control and CGD cells. The two types of H⁺ currents observed in resting and stimulated cells were activated by voltage and modulated by intra- and extracellular pH. However, the oxidase-associated currents had unique properties. First, they activated at lower voltages than known proton currents, allowing H⁺ ions to enter the cell down

their electrochemical gradient and to acidify the cytosol (Fig. 3). Second, they activated faster and deactivated much more slowly than the outward-rectifying H⁺ currents. Detailed analysis of the tail currents revealed that the slower deactivation was due to an additional kinetic component, which was absent in CGD cells (Fig. 8). Third, they were ~ 20 -fold more sensitive to Zn²⁺ and were blocked by the

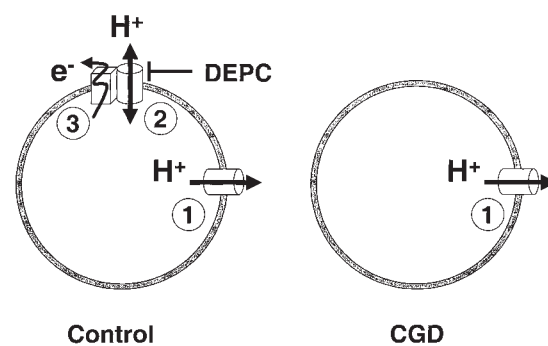


Figure 9. CGD eosinophils lack a distinct H⁺ conductance linked to the oxidase. Diagram illustrating the two types of H⁺ conductances described in this study, and their coupling to the NADPH oxidase. The “classical” H⁺ conductance (1) is present in both control and CGD cells and allows only H⁺ extrusion and repolarization. This conductance activates slowly, deactivates rapidly, is blocked by Zn²⁺ with low affinity, and is insensitive to DEPC. In contrast, the novel H⁺ conductance (2) is absent in CGD cells and allows H⁺ influx and depolarization. It activates rapidly, inactivates slowly, is highly sensitive to Zn²⁺, and is blocked by DEPC. This conductance is closely coupled to and might possibly be part of the NADPH oxidase (3).

histidine-reducing agent DEPC (Fig. 7). These distinct characteristics suggest that the oxidase-associated H^+ currents occur through a separate molecular entity (Fig. 9). In addition, block by DEPC suggests the participation of critical histidine residue(s). Interestingly, histidine-containing repeats can be found on gp91^{phox} within its third transmembrane domain, where they are thought to participate in heme binding (57). Furthermore, a recent mutagenesis study revealed that a critical histidine residue (His-115) is required for H^+ fluxes in gp91^{phox} transfectants (58). This strongly suggests that gp91^{phox} itself mediates the oxidase-associated H^+ currents, possibly through voltage-dependent translocation of protonated histidine residue(s) (53).

The H^+ channel function of NADPH oxidase had long been predicted from thermodynamic considerations (15), and was initially confirmed by pH measurement in neutrophils from CGD patients (43). Using this technique, a detailed study using different forms of CGD revealed that activation of the H^+ conductance required the assembly of the oxidase, but not its redox function (44). However, the H^+ channel function of gp91^{phox} was challenged by patch clamp detection of normal H^+ currents in monocytes from gp91^{phox}-deficient CGD patients (45). In apparent contradiction with this observation, however, gp91^{phox} was subsequently shown to confer conductive H^+ fluxes when expressed in HL-60 cells and CHO fibroblasts (40, 46).

These seemingly irreconcilable results can be fully explained by our description of oxidase-associated inward H^+ currents in activated eosinophils. The inward currents could not be detected previously, because the conditions typically used to detect H^+ currents preclude the activation of the oxidase (electron currents are not measurable under these conditions; data not shown). Therefore, most patch clamp studies relate to the endogenous outward-rectifying H^+ conductance, which is also expressed in CGD cells (Fig. 6). In this context, the presence of normal outward H^+ currents in CGD cells (45) was indeed a reasonable argument to rule out a role for gp91^{phox}. Our study confirmed that CGD cells have H^+ currents, and showed in addition that these currents can be activated by calcium and GTP γ S (Fig. 6 C). In unstimulated, acidified cells this endogenous conductance accounted for most of the H^+ current measured, and no differences could be observed between control and CGD cells (Fig. 6 B). However, in conditions favoring oxidase activation at neutral or alkaline pH_i, the oxidase-associated conductance became the predominant H^+ translocating pathway, and its defective activation in CGD cells was apparent (Fig. 6 A). Interestingly, Henderson et al. (40, 46) reported inward H^+ fluxes associated with the phagocytic H^+ conductance, an observation that was not consistent with the electrophysiological properties of the H^+ conductance. Again, this might be explained by the different conditions used, as the inward H^+ fluxes, which are not detectable in the acid patch-clamped cells, might be measurable in the alkaline intact cells.

What might be the physiological role of the oxidase-associated H^+ conductance? Its coupling to the oxidase ensures that it renders the cell membrane permeable to protons only during the respiratory burst. Because the oxidase gener-

ates an outward protonmotive force, the conductance will function, under most conditions, as an efficient proton extruder. However, the conductance also allows H^+ entry in the presence of an inward protonmotive force. Thus, at very acidic pH_o or when depolarization is blunted, such as in anoxic conditions, the conductance will favor cytosolic acidification. Since several cellular functions are inhibited at acidic pH_i (20), this might preclude microbicidal activity when phagocytes encounter acidic or anoxic environments. Indeed, earlier studies found that the FMLP- or TPA-induced respiratory burst was decreased at acidic pH_i (59, 60). This might reflect defective signal transduction or decreased NADPH production as, in our conditions, normal activity was observed at acidic pH_i when the oxidase was activated by GTP γ S and NADPH continuously perfused through the patch pipette.

In addition, changes in membrane potential caused by the oxidase-associated H^+ conductance might inhibit cellular functions, as the H^+ conductance depolarizes cells when the extracellular pH becomes more acidic than the cytosol (Fig. 1). Because the depolarization inhibits superoxide production (61), the oxidase-associated H^+ conductance might provide a negative feedback to terminate the respiratory burst in acidic environments, such as in an abscess.

Finally, the role of the oxidase-associated H^+ conductance must be considered in the context of phagocytosis. The oxidase assembles essentially around phagosomes, membrane-enclosed compartments containing the ingested microorganisms (62). The increased H^+ permeability conferred by the oxidase-associated conductance might have two important effects in phagosomes: (a) if the phagosomal membrane has a low permeability to ions other than H^+ , the oxidase will depolarize these small vesicles even more rapidly than the plasma membrane, thus opening the bidirectional H^+ conductance. Initially, H^+ entry into the phagosome (the lumen is equivalent to the extracellular space) will favor oxidase activity by preventing the depolarization. However, as the phagosomal lumen becomes more acidic than the cytosol, the H^+ conductance equilibrates the potential at progressively higher voltages (Fig. 1). As the depolarization opposes electron transport, superoxide production will decrease as phagosomes acidify. In these conditions, the NADPH oxidase-associated H^+ conductance will provide a negative feedback for the production of toxic oxygen derivatives as phagosomes mature and become more acidic. (b) If, on the other hand, the K^+ or Cl^- permeability of phagosomes is high, as has been reported in macrophages (63), changes in membrane potential are minimal and superoxide production is not affected by the acidification. In this case, the H^+ conductance will counteract the acidification by allowing H^+ efflux from the phagosome to the cytosol. Because the steady state phagosomal pH results from the equilibrium between H^+ efflux and H^+ pumping by the H^+ ATPase, the H^+ conductance will increase the phagosomal pH set point during oxidase activation. Indeed, an overshooting phagosomal acidification has been observed in granulocytes from CGD patients (64). A limitation of phagosomal acidification might be particularly relevant for granulocytes, where neutral proteases are thought to be involved in killing of phagocytosed bacteria (65).

We thank Prof. R.A. Seger and Dr. J.-P. Hossle (Kinderspital, Zurich, Switzerland) and Prof. W. Zimmerli (University Hospitals, Basel, Switzerland) for providing access to the CGD patients, and Elzbieta Huggler for expert help in the preparation of human eosinophils. We thank Drs. L. Bernheim and W. Schlegel for helpful discussions, and Dr. F. Benazilla for suggesting the DEPC experiments.

This research was funded by operating grants from the Swiss National Science Foundation (NSF) 31-46859.96, 31-45891.95, and 7UNPJ048717. N. Demaurex is a Fellow of the Dr. Max Cloetta Foundation. J. Schrenzel is the recipient of an NSF Fellowship. B. Bánfi is the recipient of a FEBS Summer Fellowship.

Address correspondence to Nicolas Demaurex, Department of Physiology, University of Geneva Medical Center, 1, Michel-Servet, CH-1211 Geneva 4, Switzerland. Phone: 41-22-702-5399; Fax: 41-22-702-5402; E-mail: Nicolas.Demaurex@medecine.unige.ch

J. Schrenzel's present address is Department of Clinical Microbiology, Mayo Clinic, Rochester, MN.

Submitted: 17 December 1998 Revised: 15 April 1999 Accepted: 19 May 1999

References

1. Babior, B.M. 1978. Oxygen-dependent microbial killing by phagocytes (first of two parts). *N. Engl. J. Med.* 298:659-668.
2. Klebanoff, S.J. 1980. Oxygen metabolism and the toxic properties of phagocytes. *Ann. Intern. Med.* 93:480-489.
3. Segal, A.W. 1981. The antimicrobial role of the neutrophil leukocyte. *J. Infect.* 3:3-17.
4. Clark, R.A. 1990. The human neutrophil respiratory burst oxidase. *J. Infect. Dis.* 161:1140-1147.
5. Segal, A.W., and A. Abo. 1993. The biochemical basis of the NADPH oxidase of phagocytes. *Trends Biochem. Sci.* 18:43-47.
6. Chanock, S.J., J. el Benna, R.M. Smith, and B.M. Babior. 1994. The respiratory burst oxidase. *J. Biol. Chem.* 269:24519-24522.
7. Segal, A.W., and K.P. Shatwell. 1997. The NADPH oxidase of phagocytic leukocytes. *Ann. NY Acad. Sci.* 832:215-222.
8. Clark, R.A. 1990. Genetic variation in chronic granulomatous disease. *Hosp. Pract.* 25:51-55, 59, 63-65 passim.
9. Boxer, L.A., and R.A. Blackwood. 1996. Leukocyte disorders: quantitative and qualitative disorders of the neutrophil, Part 1. *Pediatr. Rev.* 17:19-28.
10. Verhoeven, A.J. 1997. The NADPH oxidase: lessons from chronic granulomatous disease neutrophils. *Ann. NY Acad. Sci.* 832:85-92.
11. Ellis, J.A., A.R. Cross, and O.T. Jones. 1989. Studies on the electron-transfer mechanism of the human neutrophil NADPH oxidase. *Biochem. J.* 262:575-579.
12. Cross, A.R., and O.T. Jones. 1991. Enzymic mechanisms of superoxide production. *Biochim. Biophys. Acta.* 1057:281-298.
13. Schrenzel, J., L. Serrander, B. Bánfi, O. Nusse, R. Fouyouzi, D.P. Lew, N. Demaurex, and K.H. Krause. 1998. Electron currents generated by the human phagocyte NADPH oxidase. *Nature.* 392:734-737.
14. Henderson, L.M., J.B. Chappell, and O.T. Jones. 1988. Superoxide generation by the electrogenic NADPH oxidase of human neutrophils is limited by the movement of a compensating charge. *Biochem. J.* 255:285-290.
15. Henderson, L.M., J.B. Chappell, and O.T. Jones. 1987. The superoxide-generating NADPH oxidase of human neutrophils is electrogenic and associated with an H⁺ channel. *Biochem. J.* 246:325-329.
16. van Zwieten, R., R. Wever, M.N. Hamers, R.S. Weening, and D. Roos. 1981. Extracellular proton release by stimulated neutrophils. *J. Clin. Invest.* 68:310-313.
17. Grinstein, S., and W. Furuya. 1986. Cytoplasmic pH regulation in phorbol ester-activated human neutrophils. *Am. J. Physiol.* 251:C55-C65.
18. Borregaard, N., J.H. Schwartz, and A.I. Tauber. 1984. Proton secretion by stimulated neutrophils. Significance of hexose monophosphate shunt activity as source of electrons and protons for the respiratory burst. *J. Clin. Invest.* 74:455-459.
19. Grinstein, S., and W. Furuya. 1986. Characterization of the amiloride-sensitive Na⁺-H⁺ antiport of human neutrophils. *Am. J. Physiol.* 250:C283-C291.
20. Demaurex, N., G.P. Downey, T.K. Waddell, and S. Grinstein. 1996. Intracellular pH regulation during spreading of human neutrophils. *J. Cell Biol.* 133:1391-1402.
21. Demaurex, N., J. Orłowski, G. Brisseau, M. Woodside, and S. Grinstein. 1995. The mammalian Na⁺/H⁺ antiporters NHE-1, NHE-2, and NHE-3 are electroneutral and voltage independent, but can couple to an H⁺ conductance. *J. Gen. Physiol.* 106:85-111.
22. Thomas, R.C., and R.W. Meech. 1982. Hydrogen ion currents and intracellular pH in depolarized voltage-clamped snail neurones. *Nature.* 299:826-828.
23. Byerly, L., R. Meech, and W. Moody, Jr. 1984. Rapidly activating hydrogen ion currents in perfused neurones of the snail, *Lymnaea stagnalis*. *J. Physiol. (Lond.)* 351:199-216.
24. Barish, M.E., and C. Baud. 1984. A voltage-gated hydrogen ion current in the oocyte membrane of the axolotl, *Ambystoma*. *J. Physiol. (Lond.)* 352:243-263.
25. DeCoursey, T.E. 1991. Hydrogen ion currents in rat alveolar epithelial cells. *Biophys. J.* 60:1243-1253.
26. Demaurex, N., S. Grinstein, M. Jaconi, W. Schlegel, D.P. Lew, and K.H. Krause. 1993. Proton currents in human granulocytes: regulation by membrane potential and intracellular pH. *J. Physiol. (Lond.)* 466:329-344.
27. DeCoursey, T.E., and V.V. Cherny. 1993. Potential, pH, and arachidonate gate hydrogen ion currents in human neutrophils. *Biophys. J.* 65:1590-1598.
28. Kapus, A., R. Romanek, A.Y. Qu, O.D. Rotstein, and S. Grinstein. 1993. A pH-sensitive and voltage-dependent proton conductance in the plasma membrane of macrophages. *J. Gen. Physiol.* 102:729-760.
29. Gordienko, D.V., M. Tare, S. Parveen, C.J. Fenech, C. Robinson, and T.B. Bolton. 1996. Voltage-activated proton current in eosinophils from human blood. *J. Physiol. (Lond.)*

- 496:299–316.
30. Schrenzel, J., D.P. Lew, and K.H. Krause. 1996. Proton currents in human eosinophils. *Am. J. Physiol.* 271:C1861–C1871.
 31. DeCoursey, T.E. 1998. Four varieties of voltage-gated proton channels. *Front. Biosci.* 3:d477–d482.
 32. Lukacs, G.L., A. Kapus, A. Nanda, R. Romanek, and S. Grinstein. 1993. Proton conductance of the plasma membrane: properties, regulation, and functional role. *Am. J. Physiol.* 265:C3–C14.
 33. Demaurex, N., J. Schrenzel, M.E. Jaconi, D.P. Lew, and K.H. Krause. 1993. Proton channels, plasma membrane potential, and respiratory burst in human neutrophils. *Eur. J. Haematol.* 51:309–312.
 34. Henderson, L.M., and J.B. Chappel. 1996. NADPH oxidase of neutrophils. *Biochim. Biophys. Acta.* 1273:87–107.
 35. Susztak, K., K. Kaldi, A. Kapus, and E. Ligeti. 1995. Ligands of purinergic receptors stimulate electrogenic H(+)-transport of neutrophils. *FEBS Lett.* 375:79–82.
 36. Susztak, K., A. Mocsai, E. Ligeti, and A. Kapus. 1997. Electrogenic H⁺ pathway contributes to stimulus-induced changes of internal pH and membrane potential in intact neutrophils: role of cytoplasmic phospholipase A2. *Biochem. J.* 325:501–510.
 37. Nanda, A., and S. Grinstein. 1991. Protein kinase C activates an H⁺ (equivalent) conductance in the plasma membrane of human neutrophils. *Proc. Natl. Acad. Sci. USA.* 88:10816–10820.
 38. Kapus, A., K. Szaszi, and E. Ligeti. 1992. Phorbol 12-myristate 13-acetate activates an electrogenic H(+)-conducting pathway in the membrane of neutrophils. *Biochem. J.* 281:697–701.
 39. Qu, A.Y., A. Nanda, J.T. Curnutte, and S. Grinstein. 1994. Development of a H(+)-selective conductance during granulocytic differentiation of HL-60 cells. *Am. J. Physiol.* 266:C1263–C1270.
 40. Henderson, L.M., G. Banting, and J.B. Chappell. 1995. The arachidonate-activable, NADPH oxidase-associated H⁺ channel. Evidence that gp91-phox functions as an essential part of the channel. *J. Biol. Chem.* 270:5909–5916.
 41. Bernheim, L., R.M. Krause, A. Baroffio, M. Hamann, A. Kaelin, and C.R. Bader. 1993. A voltage-dependent proton current in cultured human skeletal muscle myotubes. *J. Physiol. (Lond.)* 470:313–333.
 42. Kaldi, K., K. Szaszi, K. Susztak, A. Kapus, and E. Ligeti. 1994. Lymphocytes possess an electrogenic H(+)-transporting pathway in their plasma membrane. *Biochem. J.* 301:329–334.
 43. Nanda, A., S. Grinstein, and J.T. Curnutte. 1993. Abnormal activation of H⁺ conductance in NADPH oxidase-defective neutrophils. *Proc. Natl. Acad. Sci. USA.* 90:760–764.
 44. Nanda, A., J.T. Curnutte, and S. Grinstein. 1994. Activation of H⁺ conductance in neutrophils requires assembly of components of the respiratory burst oxidase but not its redox function. *J. Clin. Invest.* 93:1770–1775.
 45. Nanda, A., R. Romanek, J.T. Curnutte, and S. Grinstein. 1994. Assessment of the contribution of the cytochrome b moiety of the NADPH oxidase to the transmembrane H⁺ conductance of leukocytes. *J. Biol. Chem.* 269:27280–27285.
 46. Henderson, L.M., S. Thomas, G. Banting, and J.B. Chappell. 1997. The arachidonate-activatable, NADPH oxidase-associated H⁺ channel is contained within the multi-membrane-spanning N-terminal region of gp91-phox. *Biochem. J.* 325:701–705.
 47. Hamill, O.P., A. Marty, E. Neher, B. Sakmann, and F.J. Sigworth. 1981. Improved patch-clamp techniques for high-resolution current recording from cells and cell-free membrane patches. *Pflügers Arch.* 391:85–100.
 48. Tare, M., S.A. Prestwich, D.V. Gordienko, S. Parveen, J.E. Carver, C. Robinson, and T.B. Bolton. 1998. Inwardly rectifying whole cell potassium current in human blood eosinophils. *J. Physiol. (Lond.)* 506:303–318.
 49. Cherny, V.V., V.S. Markin, and T.E. DeCoursey. 1995. The voltage-activated hydrogen ion conductance in rat alveolar epithelial cells is determined by the pH gradient. *J. Gen. Physiol.* 105:861–896.
 50. DeCoursey, T.E., and V.V. Cherny. 1994. Voltage-activated hydrogen ion currents. *J. Membr. Biol.* 141:203–223.
 51. Kaback, H.R. 1988. Site-directed mutagenesis and ion-gradient driven active transport: on the path of the proton. *Annu. Rev. Physiol.* 50:243–256.
 52. Wang, C., R.A. Lamb, and L.H. Pinto. 1995. Activation of the M2 ion channel of influenza virus: a role for the transmembrane domain histidine residue. *Biophys. J.* 69:1363–1371.
 53. Starace, D.M., E. Stefani, and F. Bezanilla. 1997. Voltage-dependent proton transport by the voltage sensor of the Shaker K⁺ channel. *Neuron.* 19:1319–1327.
 54. Miles, E.W. 1977. Modification of histidyl residues in proteins by diethylpyrocarbonate. *Methods Enzymol.* 47:431–442.
 55. Padan, E., L. Patel, and H.R. Kaback. 1979. Effect of diethylpyrocarbonate on lactose/proton symport in *Escherichia coli* membrane vesicles. *Proc. Natl. Acad. Sci. USA.* 76:6221–6225.
 56. Wang, D., D.F. Balkovetz, and D.G. Warnock. 1995. Mutational analysis of transmembrane histidines in the amiloride-sensitive Na⁺/H⁺ exchanger. *Am. J. Physiol.* 269:C392–C402.
 57. Yu, L., M.T. Quinn, A.R. Cross, and M.C. Dinauer. 1998. Gp91(phox) is the heme binding subunit of the superoxide-generating NADPH oxidase. *Proc. Natl. Acad. Sci. USA.* 95:7993–7998.
 58. Henderson, L.M. 1998. Role of histidines identified by mutagenesis in the NADPH oxidase-associated H⁺ channel. *J. Biol. Chem.* 273:33216–33223.
 59. Simchowit, L. 1985. Intracellular pH modulates the generation of superoxide radicals by human neutrophils. *J. Clin. Invest.* 76:1079–1089.
 60. Nasmith, P.E., and S. Grinstein. 1986. Impairment of Na⁺/H⁺ exchange underlies inhibitory effects of Na⁺-free media on leukocyte function. *FEBS Lett.* 202:79–85.
 61. Martin, M.A., W.M. Nauseef, and R.A. Clark. 1988. Depolarization blunts the oxidative burst of human neutrophils. Parallel effects of monoclonal antibodies, depolarizing buffers, and glycolytic inhibitors. *J. Immunol.* 140:3928–3935.
 62. Allen, L.A., and A. Aderem. 1996. Mechanisms of phagocytosis. *Curr. Opin. Immunol.* 8:36–40.
 63. Lukacs, G.L., O.D. Rotstein, and S. Grinstein. 1991. Determinants of the phagosomal pH in macrophages. In situ assessment of vacuolar H(+)-ATPase activity, counterion conductance, and H⁺ “leak”. *J. Biol. Chem.* 266:24540–24548.
 64. Segal, A.W., M. Geisow, R. Garcia, A. Harper, and R. Miller. 1981. The respiratory burst of phagocytic cells is associated with a rise in vacuolar pH. *Nature.* 290:406–409.
 65. Odell, E.W., and A.W. Segal. 1991. Killing of pathogens associated with chronic granulomatous disease by the non-oxidative microbicidal mechanisms of human neutrophils. *J. Med. Microbiol.* 34:129–135.